

Data-driven optimal filtering for phase and frequency of noisy oscillations: Application to vortex flow metering

A. G. Rossberg,* K. Bartholomé, and J. Timmer

Zentrum für Datenanalyse und Modellbildung, Universität Freiburg, Eckerstrasse 1, 79104 Freiburg, Germany

(Received 21 May 2003; published 30 January 2004)

A method for measuring the phase of oscillations from noisy time series is proposed. To obtain the phase, the signal is filtered in such a way that the filter output has minimal relative variation in the amplitude over all filters with complex-valued impulse response. The argument of the filter output yields the phase. Implementation of the algorithm and interpretation of the result are discussed. We argue that the phase obtained by the proposed method has a low susceptibility to measurement noise and a low rate of artificial phase slips. The method is applied for the detection and classification of mode locking in vortex flow meters. A measure for the strength of mode locking is proposed.

DOI: 10.1103/PhysRevE.69.016216

PACS number(s): 05.45.Tp, 06.30.Ft, 05.45.Xt

I. INTRODUCTION

Several modern methods for time series analysis make explicit use of the phase of measured oscillatory signals. Examples are tests for unidirectional [1] or mutual [2] synchronization of chaotic oscillators, based on accurate or noisy [3] data, identification of the coupling direction [4,5], or indicators [6] for generalized synchronization [7]. Phase analysis has successfully been applied in neurology [8–10], cardiology [3,5,11,12], ecology [13], and astronomy [14] and laser physics [15] (for recent, comprehensive reviews, see Refs. [16,17]).

A number of ways have been proposed to measure the phase from univariate signals. Among these are (a) phase determination from the argument of the analytic signal [18], from the convolution of the signal with a Morlet wavelet [15,19], or after complex demodulation or quadrature filtering [20], (b) the angle of circulation of a two-dimensional (2D) projection of the reconstructed phase-space trajectory [17] or its time derivative [21] around a point; and (c) linear interpolation [1] of phase between distinct events marking the beginning new cycles [17].

In principle, the problem of choosing the most appropriate method to obtain the phase has two aspects: First, defining phase for the oscillator under investigation and, second, estimating this phase from an univariate signal which is typically biased by noise. While for autonomous, noise-free limit-cycle oscillators the definition of phase has a natural and rigorous foundation, there is no obvious unique generalization of this concept to oscillators deviating from this ideal, e.g., due to internal noise or chaotic dynamics. Presumably, those measures of phase are to be given preference which lead to the most distinctive characterizations of the observed systems [22]. Of course, with increasing deviations from the ideal of a periodic oscillator, there are less merits in using the concept of phase.

When the phase is to be estimated from an univariate

signal, knowledge about the oscillator and the contribution of the oscillator and other processes to the signal is often poor. Thus, systematically deriving estimators for particular definitions of phase is possible only in a few exceptional cases. Instead, the measure of phase is again chosen by the distinctiveness of the resulting characterization [9,15,23]. Thereby it is generally assumed correctly that, if the phase-space trajectory of the oscillator was directly accessible, an improved measure of phase that leads to more distinctive characterizations could be obtained.

Although some rules for selecting a method to measure phase for a given signal have been proposed [17], the choice is not always obvious. The wish list for properties of the phase $\phi(t)$ includes a constant advance of 2π per cycle, a steady accumulation [$\dot{\phi}(t) \approx \text{const}$], accuracy in the presence of measurement noise, unambiguity with respect to 2π phase slips, and a functional dependence on the current state of the oscillator (locality). Autonomy of the oscillator combined with steady accumulation and locality of phase implies that $\phi(t)$ is the variable that corresponds to the zero Lyapunov exponent of the system—another desired property.

But only for perfectly periodic signals can all these wishes be fulfilled. For deterministic, chaotic oscillators the linear-interpolation method (c) does often lead to a satisfactory steady and local phase. The problem of defining a steady, local phase when the internal dynamics of a deterministic, chaotic oscillator are known was treated rigorously in Ref. [24]. But as internal and measurement noise become stronger, some temporal averaging is required and locality in time has to be traded for accuracy and/or unambiguity. In Refs. [3,5,8,11–14] the condition of unambiguity was relaxed and only the cyclic phases [$\phi(t) \bmod 2\pi$] of noisy oscillations were used. Thus data analysis was insensitive to phase slips, i.e., sudden advances of the phase by $\pm 2\pi$, which may or may not be artifacts of measurement noise. Here we choose to be less demanding with respect to locality, in favor of a steady, accurate and, as much as possible, unambiguous phase.

In order to identify a corresponding method to measure the phase, notice that the computation of the analytic signal (or complex demodulation) [method (a)] is generally recom-

*Electronic address: rossberg@uni-freiburg.de; URL: <http://www.fdm.uni-freiburg.de>

mended to be combined with linear bandpass filtering of the desired oscillatory component [20,25]. The overall effect is the application of a complex-valued, linear bandpass filter [15]. When the method of delays is used for the phase-space reconstruction of the angle-of-circulation method (b), the 2D projection is also equivalent to complex-valued linear filtering [26], likewise the calculation of time derivatives.

Finally, in the vicinity of a Hopf bifurcation, where dynamics can be brought into Hopf normal form by a nonlinear coordinate transformation (see, e.g., Ref. [27]), this transformation is done in such a way that all contributions to dynamics which are “nonresonant” with the oscillation at the fundamental frequency are eliminated. In mere *kinetic* terms this simply amounts to eliminating higher harmonics and offsets, which can be achieved by complex, linear bandpass filtering. The SU(2) symmetry of the Hopf normal form guarantees the steady accumulation of phase in the steady state, when phase is measured as the angle of rotation around the origin.

Thus, a unified view on (a) and (b) is complex, linear bandpass filtering. It achieves steady accumulation in a natural way when the fundamental mode is isolated. The results regarding accuracy and unambiguity depend on the choice of the filter. Since the concept of phase originates from limit-cycle oscillations, which, in the transformed coordinates, correspond to a motion on a circle, our idea for choosing the filter here is to make the filtered signal move as close as possible to a circle in the complex plane. Roughly speaking, we consider the motion on the circle as the signal and the deviations as noise and maximize the signal to noise ratio (SNR)—even though not all deviations are actually due to measurement noise. Since, with such a filter, noise-induced excursions of the trajectory to the origin of the complex plane are minimized, this is also a good way to reduce ambiguities in the phase. The maximization of the SNR is done not only with respect to width and center frequency of the filter, but with respect to the complete dynamics of its impulse response. The determination of the filter is nonparametric and data driven.

We proceed as follows. Section II contains a mathematical formulation of the ideas outlined above and lists some implications. In Sec. III the method is applied to simulated data, with special attention to the effect of filtering on measured frequencies. A practical application to vortex flow meters is discussed in Sec. IV, where we also introduce a measure for the strength of mode locking.

II. THEORY

A. MIRVA filters

1. Definition

Let $x(t)$ be a real- or complex-valued stationary signal with oscillatory components. Denote by $z(t)$ the signal obtained from $x(t)$ by linear filtering with a complex-valued filter with impulse response $f(t)$, i.e., $z = f * x$ where “*” indicates convolution. Define q as the non-negative number such that

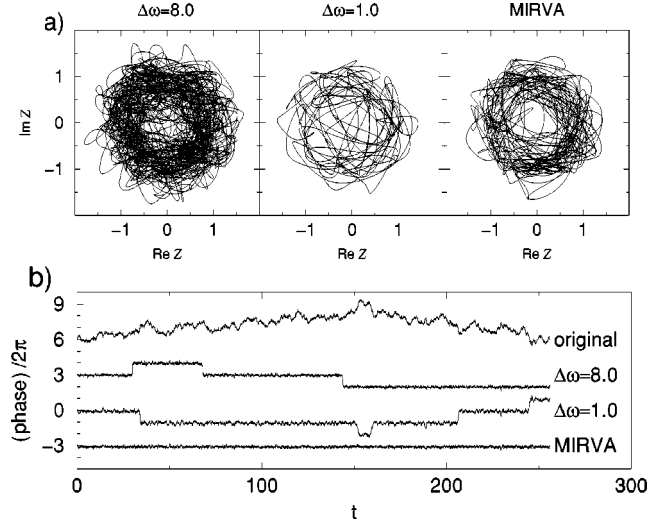


FIG. 1. Three different filters applied to the same time series (2). (a) The demodulated, filtered signals $Z(t) = z(t)\exp(-i\omega_0 t)$. (b) The phase $\phi_0(t) - \omega_0 t$ of the original signal and the relative phases $\phi(t) - \phi_0(t)$ obtained using the three filters. See text for details.

$$q^2 = \frac{\text{var}|z|^2}{\langle |z|^2 \rangle^2} = \frac{\langle |z|^4 \rangle}{\langle |z|^2 \rangle^2} - 1, \quad (1)$$

where $\langle \cdot \rangle$ denotes the expectation value.

Now, search for a filter f such that the quantity q given by Eq. (1) has a local minimum with respect to the filter. Such a filter f minimizes the relative variance of the amplitude (MIRVA) for the given signal $x(t)$. The practical computation of MIRVA filters is addressed in Appendix A.

For every MIRVA filter f , there is a two-parameter family of MIRVA filters $f_{s,c}(t) = cf(t-s)$ with real s and complex c . Below we shall always have a single member stand for the whole family without saying.

2. Example

As an example, assume that $x(t)$ is composed of a constant-amplitude oscillation with phase fluctuations and white measurement noise,

$$x(t) = \cos[\omega_0 t + \phi_0(t)] + \eta(t), \quad (2)$$

where

$$\langle \phi_0(t)\phi_0(t') \rangle = 2D\delta(t-t'), \quad \langle \eta(t)\eta(t') \rangle = 2G\delta(t-t'). \quad (3)$$

This signal mimics narrow-banded limit-cycle and chaotic oscillations in the vicinity of the fundamental frequency. The larger the noise strength G , the more difficult the determination of the phase $\phi_0(t)$ from $x(t)$ becomes. We simulate $x(t)$ with $D = 1$, $G = 0.01$, and $\omega_0 = 20$ over an interval of length $T = 256$. Without any filtering, the SNR is zero. Figure 1(a) shows the demodulated signals $Z(t) = z(t)\exp(-i\omega_0 t)$ for three different complex filters $f(t)$. The first two filters are of the form

$$f(t) \sim \exp[i\omega_0 t - \frac{1}{2}(\Delta\omega t)^2]. \quad (4)$$

One is a comparatively wide ($\Delta\omega=8.0$) bandpass, the other one is rather narrow ($\Delta\omega=1.0$). The third is the MIRVA filter obtained by minimizing Eq. (1). It is approximated by Eq. (4) with $\Delta\omega=2.9$. As is shown in Fig. 1(b), both the narrow and the wide filter lead to artificial phase slips. Only when using the MIRVA filter is $\phi_0(t)$ faithfully tracked.

3. Remarks on the minimization of q

Let q_{\min} denote the value of q attained at a local minimum. Since the operation of linear filtering defines a semigroup, q_{\min} is also a local minimum of q with respect to further filtering of $z(t)$, i.e., for q calculated with z replaced by $z' := g * z$. The minimum is attained when the filter g is the unit element of the semigroup, the Dirac δ function. As a result one has

$$0 = \left. \frac{1}{2} \frac{\delta q^2}{\delta g(\tau)} \right|_{g=\delta} = \frac{\langle |z(t)|^2 \bar{z}(t) z(t-\tau) \rangle \langle |z(t)|^2 \rangle - \langle |z(t)|^4 \rangle \langle \bar{z}(t) z(t-\tau) \rangle}{\langle |z(t)|^2 \rangle^3} \quad (5)$$

for all τ . In particular, when differentiating with respect to τ at $\tau=0$ and taking the imaginary part, it follows that

$$\frac{\langle |z|^4 \omega_i \rangle}{\langle |z|^4 \rangle} = \frac{\langle |z|^2 \omega_i \rangle}{\langle |z|^2 \rangle} = \omega_{\text{mean}}, \quad (6)$$

where ω_i is the instantaneous frequency defined by

$$\omega_i := \text{Im} \left\{ \frac{\dot{z}}{z} \right\} \quad (7)$$

and ω_{mean} is known as the *mean frequency*, defined either by the last equation of Eq. (6) or, equivalently, as the ‘‘center of mass’’ of the power spectrum of the signal z . For the relation of the mean frequency to the *phase frequency* (or average frequency) $\omega_{\text{ph}} := \langle \omega_i \rangle$ see Sec. III.

Often, signals contain oscillations at several different frequencies. A systematic method to extract various oscillation frequencies has been proposed in Ref. [28]. When using the concept of MIRVA filtering, distinct local minima of q can be identified with distinct oscillatory components of the signal.

4. Special cases

In two special cases the problem of finding MIRVA filters can be discussed analytically. For perfectly periodic or quasiperiodic signals there is, for every Fourier mode excited by the signal, a MIRVA filter that extracts exactly this mode. The filtered signal is of the form $z(t) = \exp(i\omega t)$ and $q_{\min} = 0$. This holds true also if the signal is overlaid by any kind of noise.

For Gaussian, linear processes it is always possible to find filters such that $\langle z^2 \rangle = 0$ and $\langle |z|^2 \rangle \neq 0$, e.g., by letting only Fourier modes with positive frequency pass. Then $\langle |z|^4 \rangle = 2\langle |z|^2 \rangle^2$, $q = q_{\min} = 1$, and all these filters are MIRVA filters.

The processes we are interested in here are typically located between these two poles: noisy, nonlinear, periodic processes with some fluctuations in the phase. Thus we expect $0 < q_{\min} < 1$. When solving the optimization problem $q^2 = \min$ numerically with time series of finite length T (see Appendix A), local minima with $q_{\min} > 1$ have also been

found. It is not clear whether these persist in the limit $T \rightarrow \infty$.

B. The phase of MIRVA filtered signals

1. Definition and error estimates

The main purpose of MIRVA filtering is to obtain the phase

$$\phi(t) = \int^t \omega_i(t') dt' \equiv \arg z \pmod{2\pi} \quad (8)$$

of the oscillations extracted by the filter.

In order to analyze the effect that the contribution of measurement noise $\eta(t)$ to $z(t)$ has on the measured phase $\phi(t)$, denote by $z_0(t) := z(t) - \eta(t)$ the noise-free component of $z(t)$, and the phase that would have been measured in the absence of measurement noise by $\phi_0(t) := \int^t \text{Im} \{ \dot{z}_0(t') / z_0(t') \} dt'$. Two kinds of errors in $\phi(t)$ caused by measurement noise can be distinguished: deviations by multiples of 2π , i.e., phase slips, which are due to noise-induced excursions of $z(t)$ around the origin and accumulate as time proceeds, and errors in the cyclic phase $[\phi(t) - \phi_0(t) + \pi] \pmod{2\pi} - \pi$, which have a finite correlation time. The distinction is particularly sharp when q_{\min} is small enough, so that the probability density for values of $z(t)$ near zero is small, or, as we shall consider now, when q is small for general filters f .

An order-of-magnitude estimate for an upper bound to the rate of noise-induced phase slips is given by

$$p \left[\frac{|z|^2}{\langle |z|^2 \rangle} = 0 \right] \Delta\omega, \quad (9)$$

where the first term denotes the probability density of $|z|^2 / \langle |z|^2 \rangle$ at zero and the second term denotes the spectral width of the filter. The first term typically decays exponentially fast as q^2 decreases, while the relation between q^2 and $\Delta\omega$ is only algebraic in general. Hence, minimizing q^2 is a good strategy to minimize phase slips.

For the noise-induced error in the cyclic phase, an exact upper bound can be obtained in the limit that q^2 is small. For simplicity, assume that the noise has undergone sufficient temporal averaging by the filter f , so that the central limit theorem applies and $\eta(t)$ is Gaussian. Since f is a complex bandpass filter, $\langle \eta^2 \rangle = 0$. In order to derive an upper bound for $\langle |\eta|^2 \rangle$ from q^2 , we assume the worst case, that is, all variation in $|z|^2$ is due to η only, while $|z_0|^2 \equiv \text{const} = 1$ without loss of generality. For limit-cycle oscillators the resulting upper bound is attained. In the general case, including chaotic oscillators, a conservative estimate of the noise intensity is obtained.

Since η is independent of z_0 , Eq. (1) can then be written as

$$q^2 = \frac{1 + 4\langle |\eta|^2 \rangle + 2\langle |\eta|^2 \rangle^2}{1 + 2\langle |\eta|^2 \rangle + \langle |\eta|^2 \rangle^2} - 1. \quad (10)$$

Solving for $\langle |\eta|^2 \rangle$ yields

$$\langle |\eta|^2 \rangle = (1 - q^2)^{-1/2} - 1 = \frac{q^2}{2} + O(q^4). \quad (11)$$

The corresponding noise-induced variance in ϕ is

$$\begin{aligned} \text{var } \phi &= \text{var}[\arg(z_0 + \eta) - \arg(z_0)] \\ &= \text{var}\left[\arg\left(1 + \frac{\eta}{z_0}\right)\right] \\ &= \text{var}\left[\text{Im}\left\{\frac{\eta}{z_0}\right\}\right] + O(\langle |\eta|^2 \rangle^2) \\ &= \frac{\langle |\eta(t)|^2 \rangle}{2} + O(\langle |\eta|^2 \rangle^2). \end{aligned} \quad (12)$$

In the general case, when $|z_0|$ is not constant, we get, from combining Eqs. (11) and (12),

$$\text{var } \phi \leq \frac{q^2}{4} + O(q^4). \quad (13)$$

Thus, minimizing q^2 is a good strategy to minimize noise-induced errors in the measured cyclic phases.

2. Phase diffusion

Over long time intervals, $\phi(t)$ typically performs a random walk with drift. Thus, an important characteristic of the phase is its diffusion coefficient

$$D := \lim_{T \rightarrow \infty} \frac{\langle \phi(t+T) - \phi(t) - \omega_{\text{ph}}T \rangle}{2T}. \quad (14)$$

The estimation of D from finite-length samples of $\phi(t)$ is discussed in Appendix B.

C. Invariance with respect to filtering of $x(t)$

The MIRVA filtered signal $z(t)$ and the phase and frequency derived thereof are invariant with respect to linear

filtering of the original signal $x(t)$ in the following sense. Let $y(t)$ be a signal obtained from $x(t)$ by linear filtering, i.e., $y = h*x$, and let f be a MIRVA filter for x . Then, a MIRVA filter for y is, at least formally, given by $f' = f*h^{-1}$, where h^{-1} is the inverse of h defined by $h^{-1}*h = \delta$. So the filtered signal $z = f*x = f'*y$ which satisfies the minimization condition (5) is identical for x and y . For example, MIRVA filtering can be used to obtain the phase and frequency of an oscillatory signal which has been “bleached” [29], i.e., filtered such as to make its power spectrum white (see Ref. [30]).

The concept of MIRVA filtering carries straightforwardly over to a discrete-time representation of signals x_i , z_i and filters f_k , sampled at time intervals of length Δt . In Ref. [30] the notion of a *topological frequency* of a time-discrete signal x_i is defined. Roughly speaking, this is the rate of transitions of the trajectory of the signal in a sufficiently high-dimensional delay space through a particular kind of Poincaré section called a *counter*. For the topological frequency, the invariance with respect to linear filtering has been proven rigorously [30]. When the modulus of the signal z_i obtained by MIRVA filtering a signal x_i and its linear interpolation have a nontrivial lower bound, i.e., $|l z_i + (1-l) z_{i+1}| > d > 0$ for $0 \leq l \leq 1$, and when the impulse response f_k of the MIRVA filter decays sufficiently fast for large k , then ω_{ph} obtained from z_i and its linear interpolation is (up to the sign) identical to a topological frequency of the oscillations of the signal x_i . A corresponding counter can be obtained as follows. Assume that all significant contributions to f_k are within a range of M consecutive delay times. Then the filter operation $f*x$ can be interpreted as a projection from the M -dimensional delay space of x_i into the two-dimensional complex plane. The counter is given by all points in delay space which are projected onto the real, non-negative half axis.

III. THE EFFECT OF MIRVA FILTERING ON MEASURED FREQUENCIES

In order to illustrate the effects of MIRVA filtering on measured frequencies, the method is applied to a numerical solution of the noisy Stuart-Landau equation (or Hopf normal form)

$$\dot{A} = (\epsilon + i\omega_l)A - (g_r + i g_i)|A|^2 A + \zeta, \quad (15)$$

where $A = A(t)$ represents the complex amplitude of an oscillator and $\zeta(t)$ is complex-valued, Gaussian, white noise with correlations

$$\langle \zeta(t)\zeta(t') \rangle = 0 \quad \text{and} \quad \langle \zeta(t)\bar{\zeta}(t') \rangle = 4G\delta(t-t'). \quad (16)$$

In a certain sense, this system universally describes noisy oscillations in the vicinity of a Hopf bifurcation [31]. Assume the bifurcation to be supercritical ($g_r > 0$) and do a linear change of coordinates to set $g_r = G = 1$ and $\omega_l = 0$ without loss of generality (even though, in practice, $\omega_l \gg \epsilon$). When $g_i \neq 0$, the phase frequency,

$$\omega_{\text{ph},A} = -g_i(\epsilon + 2\mathcal{N}^{-1}) \quad (17)$$

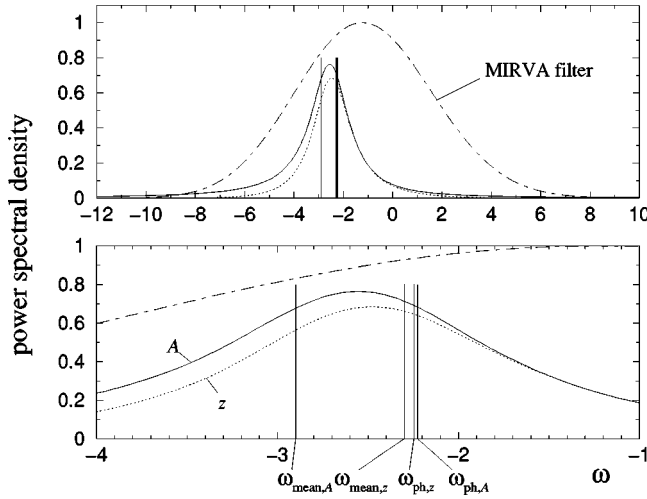


FIG. 2. MIRVA filtering of the process $A(t)$ given by Eqs. (15) and (16) with $\omega_i=0$, $g_r=g_i=G=1$, and $\epsilon=2$. The lower graph is a blowup of the upper graph. Both show the power spectral density of $A(t)$ (solid), of the filtered signal $z(t)$ (dotted), and the characteristics of the MIRVA filter (dash-dotted). The vertical lines indicate the locations of various frequencies associated with the process.

(where $\mathcal{N} := \pi^{1/2} \exp(\epsilon^2/4)[1 + \text{erf}(\epsilon/2)]$, see, e.g., Refs. [30,32]), calculated from $\omega_{i,A} = \text{Im}\{\dot{A}/A\}$ directly without filtering, differs from the corresponding mean frequency

$$\omega_{\text{mean},A} = -g_i[2\epsilon^{-1} + \epsilon - 4(2\epsilon + \epsilon^2\mathcal{N})^{-1}]. \quad (18)$$

This is a direct consequence of the correlation between $\omega_{i,A}$ and $|A|^2$ ($\langle \omega_{i,A}|A|^2 \rangle / \langle |A|^2 \rangle \neq \langle \omega_{i,A} \rangle$).

As an example, a simulation of $A(t)$ of length $T=10^6$ with $\epsilon=2$ and $g_i=1$ is generated using Euler steps of length 2^{-11} . For these parameters, $\omega_{\text{ph},A} = -2.225$, $\omega_{\text{mean},A} = -2.899$, and the relative variance of the unfiltered amplitude is $\langle |A|^4 \rangle / \langle |A|^2 \rangle^2 - 1 = (2\mathcal{N}^2 - 2\epsilon\mathcal{N} - 4) / (\epsilon\mathcal{N} + 2)^2 = 0.303$.

The MIRVA filter for the time series $x(t)=A(t)$ is calculated by the indirect method described in Appendix A. The filter reduces the relative variance of the amplitude to $q_{\text{min}}^2 = 0.164$. Figure 2 shows the characteristics of the MIRVA filter in comparison with the power spectrum of the original signal $A(t)$ and the filtered signal $z(t)$. The locations of phase and mean frequency before filtering and after filtering [$\omega_{\text{ph},z} = -2.245(2)$, $\omega_{\text{mean},z} = -2.298(2)$] are also indicated. The MIRVA filter is a rather wide (half width $2\Delta\omega \approx 6.5$), approximately symmetric bandpass filter with a center frequency $\omega_c \approx -1.3$ below the linear frequency $\omega_l = 0$. As a result, the phase frequency of the filtered signal is also shifted to lower frequencies, but the effect $\omega_{\text{ph},z} - \omega_{\text{ph},A} \approx -0.02 = O(\Delta\omega^{-1}\mathcal{N}^{-1}\omega_c)$ (see Ref. [30]) is quite small.

On the other hand, there is a pronounced shift in the mean frequency by MIRVA filtering: the mean frequency approaches the phase frequency. This is a generic effect of MIRVA filtering. In the presence of a negative correlation between amplitude and instantaneous frequency, as found in our example, a filter that amplifies the signal when ω_i is high

and damps the signal when ω_i is low reduces fluctuations in the amplitude and, at the same time, reduces the correlation. Since the phase frequency is only weakly affected by MIRVA filtering, the mean frequency is shifted toward the phase frequency.

IV. APPLICATION TO VORTEX FLOW METERING

A. Background

Next, an application of MIRVA filters to vortex flow metering is discussed. Vortex flow meters are widely used in the industry to measure pipe flow. The measurement principle makes use of the phenomenon of the von-Kármán vortex street. Behind a shedder bar inserted normal to the flow in a pipe, a regular chain of vortices is formed, rotating alternately left and right. The volume flow through the tube can be determined from the frequency of vortex formation. In the device used here, a piezoelectric sensor sensitive to transversal flow, which is inserted downstream behind the shedder bar, is used to detect the vortices passing by. A common problem of vortex flow metering is mode locking of the vortex oscillations to pulsations in the flow. The second-order statistics (power spectra) of the sensor signal and the bias on the flow measurement in the presence of mode locking have been thoroughly investigated [33]. But it seems possible that, by processing the sensor signal with a stronger focus on the nonlinear dynamics of the system, a better control of mode locking can be achieved.

Here we describe the analysis of time series recorded in an experiment designed to simulate the problem of detecting mode locking in an industrial context, using only the sensor signal. Methods that have been proposed to detect mode locking from univariate time series are the analysis of the map of subsequent period lengths of the oscillation (angle-of-return-times-map) [34] and the application of the established bivariate methods on pairs of time series extracted from the univariate series by filtering [35]. We go along the lines of the second approach, making it more powerful by applying MIRVA filters to separate the signals.

The setup of the experiment is sketched in Fig. 3. Pulsations of the pipe flow were generated by a rotating cylinder with three bores orthogonal to the cylinder axis, which is inserted into the pipe in such a way that, by the rotation, the flow is periodically blocked. This pulsator is driven by an electric motor. The sensor signal of a commercial flow meter, which was mounted about 40 pipe diameters downstream from the pulsator, was recorded. Estimates of the pulsation rate ν_{puls} and the frequency of vortex formation ν_{vort} were available on-site, while recording the time series. Reynolds numbers were $O(10^5)$ and the flow was highly turbulent. As a result, both inherent and measurement noise contribute substantially to the signal. Details of the experimental setup will be reported elsewhere. Below, two experimental time series labeled as A and B are discussed. Both were recorded from the sensor of the vortex flow meter at 2 kHz over 250 s.

B. Series A: hard lock-in

1. Determination of the phases

When recording series A, the flow rate was adjusted such as to obtain $\nu_{\text{vort}} \approx 110$ Hz and the pulsation frequency was

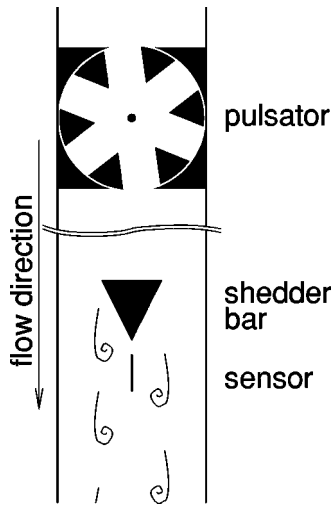


FIG. 3. Schematic representation of the experimental setup to record the sensor signal of a vortex flow meter in pulsatile flow. The shedder bar has a triangular cross section for efficient vortex generation.

set to $\nu_{\text{puls}} \approx \frac{2}{3} \nu_{\text{vort}}$. The time series was analyzed to determine the strength of the expected 2:3 lock-in. In Fig. 4, a representative section of series A and the power spectrum are shown. The oscillations at ν_{vort} can clearly be seen. Since the pulsations themselves do not produce any transversal flow, there is only a weak signal at ν_{puls} , presumably due to slight asymmetries in the setup. By the nonlinear interaction of vortex street and pulsation, flow oscillations at $\nu_{-} = \nu_{\text{vort}} - \nu_{\text{puls}}$ are excited. These contain significant transversal components and can clearly be seen in the power spectrum. The power spectrum also reveals several other oscillatory components in the signal. Some of these are nonlinearly generated, others are of unknown origin.

The impulse response of the MIRVA filter for the 110 Hz vortex oscillations (ν_{vort}) is shown in Fig. 5. It was calculated by the indirect method described in Appendix A using a

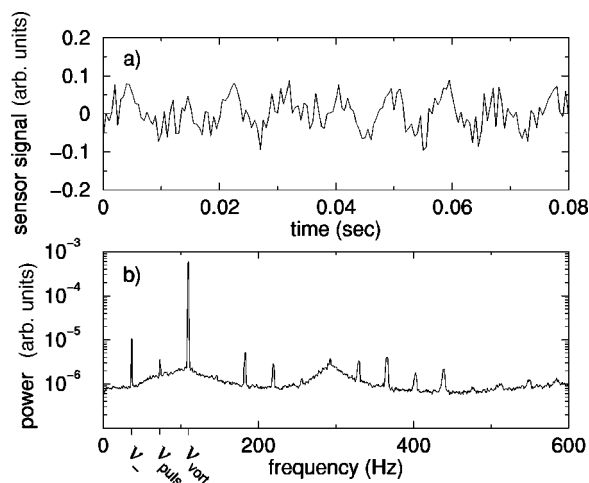


FIG. 4. A representative section (a) and the power spectral density (b) of time series A, which was recorded in the experiment sketched in Fig. 3.

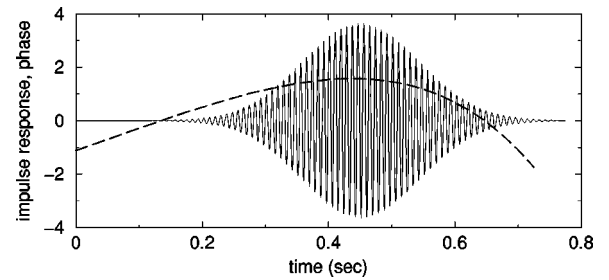


FIG. 5. The impulse response $f(t)$ of the MIRVA filter calculated for series A at the frequency ν_{vort} . Solid, $\text{Re}\{f(t)\}$; dashed, phase of $f(t)$, relative to an oscillation at constant frequency $\omega_0/2\pi = 109.64$ Hz, i.e., $\arg[f(t)\exp(-i\omega_0 t)]$. The overall offset in time is an accidental choice of the search algorithm.

down-sampling factor $h = 50$, $M = 30$ sampling points, a demodulation frequency $\omega_0/2\pi = 109.643$ Hz, and a regularization by $m = 10$ th order polynomials. The overall Gaussian shape of the impulse response of the MIRVA filter can clearly be seen. But the filter has additional structure. The oscillation frequency of the response function decreases with time (see the phase in Fig. 5). The reason for this particular phase dynamics is not clear by now. As can be seen from the trajectory of the demodulated filtered signal Z_i shown in Fig. 6 (right), the phase of the vortex oscillations is always well defined.

From the construction of the pulsator it is clear that the flow pulsations have a well defined phase. Each passage of a bore along the pulsator inlet (or outlet) defines one pulse. But the signal-to-noise ratio of the oscillations at ν_{puls} is too low to derive unequivocal phase information. As is shown in Fig. 6 (center), the MIRVA filtered signal at ν_{puls} repeatedly reaches the origin of the complex plane.

In contrast, the phase of the oscillations at ν_{-} is much better defined (see Fig. 6, left). Since the signal-to-noise ratio is smaller at ν_{-} than at ν_{vort} , the MIRVA filter at ν_{-} is about eight times more narrow in Fourier space than the MIRVA filter at ν_{vort} . Use of the MIRVA filter (or some approximation) is critical for measuring the phase at ν_{-} . Here, straightforward boxcar filtering of a region in Fourier space containing the ν_{-} peak (see, e.g., Ref. [35]) would be insufficient.

The phase ϕ_{-} of the oscillations at ν_{-} can be used to determine the phase ϕ_{puls} of the pulsator. By the physical

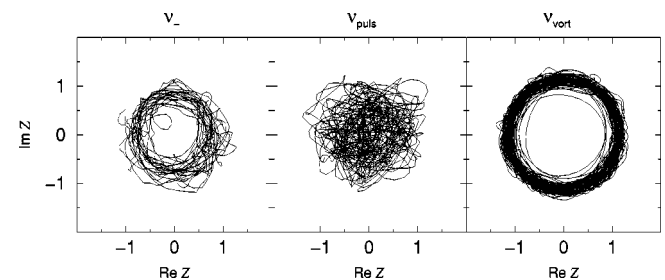


FIG. 6. The trajectories of demodulated, MIRVA filtered signals Z_i (see section 2 of Appendix), obtained from series A at the indicated frequencies. The corresponding values of q_{min} are 0.41 (ν_{-}), 0.81 (ν_{puls}), and 0.13 (ν_{vort}).

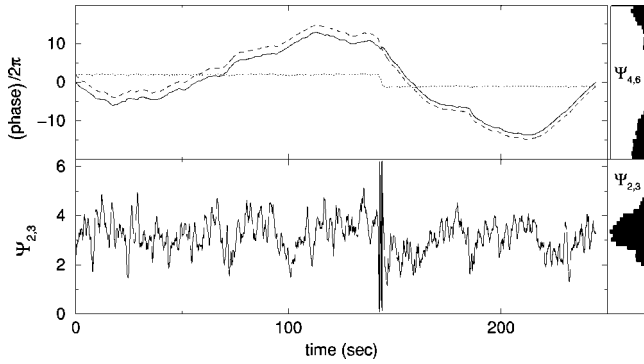


FIG. 7. Phases, obtained from series A. Large upper panel: the unwrapped phases $3\phi_{-}(t) - \omega_0 t$ (solid) and $\phi_{\text{vort}}(t) - \omega_0 t$ (dashed), where $\omega_0/2\pi = 109.654$ Hz (nominal value); $\phi_{2,3} = 3\phi_{-} - \phi_{\text{vort}}$ (dotted). Large lower panel: the cyclic relative phase $\Psi_{2,3}$. Small panels: empirical distributions of $\Psi_{4,6}$ and $\Psi_{2,3}$.

interpretation of the oscillation at ν_{-} as a nonlinear excitation, one has the relation

$$\phi_{-} = \phi_{\text{vort}} - \phi_{\text{puls}} \quad (19)$$

that yields ϕ_{puls} for known ϕ_{-} and ϕ_{vort} .

2. Relative phases and symmetry

From the 2:3 mode locking, one expects that the relative phase $\phi_{2,3}$, given by

$$\phi_{n,m} := n\phi_{\text{vort}} - m\phi_{\text{puls}}, \quad (20)$$

changes only little over time. For hard mode locking, it fluctuates around a constant value. With both hard and soft lock-in, the cyclic relative phase $\Psi_{2,3}$ defined by

$$\Psi_{n,m} := \phi_{n,m} \bmod 2\pi \quad (21)$$

has an uneven distribution. Generally, one expects the distribution to be increasingly sharper localized to a single value as mode locking becomes stronger. The synchronization index defined in Ref. [36] as

$$\gamma_{n,m}^2 := \langle \cos \Psi_{n,m} \rangle^2 + \langle \sin \Psi_{n,m} \rangle^2 \quad (22)$$

with expectation values estimated by temporal averaging, was therefore proposed as a measure for the strength of mode locking or, more general, phase locking. Absence of mode locking is indicated by $\gamma_{n,m} = 0$, hard coupling by $\gamma_{n,m} = 1$. In our experiment, we encounter the particular situation that vortices and pulsation have opposite symmetries with respect to transversal reflection. Thus, dynamics is equivariant already with respect to a shift of ϕ_{vort} by π , rather than 2π . Ideally, one would therefore always expect $\gamma_{2,3}^2 = 0$, with or without mode locking. In order to take this degeneracy into account, $\gamma_{4,6}^2$ should be used instead of $\gamma_{2,3}^2$.

3. Interpretation of the measured phases

The evolution of the measured values for ϕ_{-} and ϕ_{vort} , and of the relative phase $\phi_{2,3} = 2\phi_{\text{vort}} - 3\phi_{\text{puls}} = 3\phi_{-} - \phi_{\text{vort}}$ is shown in Fig. 7. Since the definition of MIRVA

filters leaves the overall delay of the filtered signal undetermined, the relative delay of ϕ_{-} and ϕ_{vort} has to be adjusted in a reasonable way. We choose the delay such that $\gamma_{2,3}$ becomes maximal ($\gamma_{2,3}$ turns out not to vanish, see below). From the evolution of $\phi_{2,3}$ it appears that the vortex oscillations contain only a single phase slip at about 150 s into the time series. But upon closer inspection, it appears more plausible to account the phase slip to an error in measuring ϕ_{-} . As expected for this case, the difference in $\phi_{2,3}$ before and after the slip is to a good accuracy 6π . For slips in ϕ_{vort} , any other multiple of π would have been possible as well. Furthermore, the slip occurs just at the moment when the demodulated MIRVA signal at ν_{-} (Fig. 6, left) goes through the small loop reaching toward the coordinate center. It appears that the MIRVA filter is too narrow for the comparatively low pulsation frequency at this moment. In fact, the phase slip disappears when wider filters are used—at the price of obtaining new artificial phase slips at other times. In conclusion, the data indicate that there is not a single real phase slip. Lock-in is hard over the full 250 s sampling time.

The relevant synchronization index $\gamma_{4,6}^2 = 0.16$ is much smaller than one would expect for hard mode locking (see also the distributions of $\Psi_{4,6}$ in Fig. 7). Use of a synchronization index based on Shannon entropy [3] yields a similar result. Even when the transversal reflection symmetry was strongly broken, the then relevant synchronization index $\gamma_{2,3}^2 = 0.62$ would be rather low. But, as can be seen from Fig. 10 below, the symmetry is only weakly broken. A natural explanation for the discrepancy between the synchronization index and the phase-slip statistics is to assume that most of the fluctuations in $\Psi_{2,3}$, respectively, $\Psi_{4,6}$ (Fig. 7; $\Psi_{4,6} = 2\Psi_{2,3} \bmod 2\pi$), are due to measurement noise, and not intrinsic to the vortex dynamics. This view is compatible with the upper bound derived for the variance due to noise in Sec. II B. From $q_{-} := q_{\text{max}} = 0.41$ at ν_{-} and $q_{\text{vort}} := q_{\text{max}} = 0.13$ at ν_{vort} , one gets the approximate upper bound $3^2 q_{-}^2/4 + q_{\text{vort}}^2/4 = 0.38$ for the variance contributed to $\Psi_{2,3}$ by measurement noise, while the total variance is $\text{var}\Psi_{2,3} = 0.48$. It appears that, in some situations, a characterization of mode locking by phase-slip statistics is less susceptible to measurement noise than characterizations based only upon cyclic phases, i.e., quantities such as $\phi_{\text{puls/vort}} \bmod 2\pi$ or, computable thereof, $\Psi_{4,6}$.

C. Series B: Soft lock-in

1. Determination of the phases

Series B was recorded with $\nu_{\text{vort}} \approx 110$ Hz and $\nu_{\text{puls}} \approx 55$ Hz and 1:2 mode locking is expected. Similar as for series A, MIRVA filtering readily yields the unwrapped phase ϕ_{vort} of the oscillation $\sim \exp(i\phi_{\text{vort}})$ at ν_{vort} (Fig. 8, right). We assume that, as for series A, the oscillations $\sim \exp(i\phi_{\text{puls}})$ due to pulsation alone are much weaker than the oscillations $\sim \exp(i\phi_{\text{vort}} - i\phi_{\text{puls}})$ excited by nonlinear interaction of vortices and pulsation. Thus, the nonlinear excitation dominates the oscillations at $\nu_{\text{puls}} \approx \nu_{-} := \nu_{\text{vort}} - \nu_{\text{puls}}$. In contrast to series A, MIRVA filtering at ν_{-} does not lead to an unequivocal phase (Fig. 8, center). It appears that this is due to phase

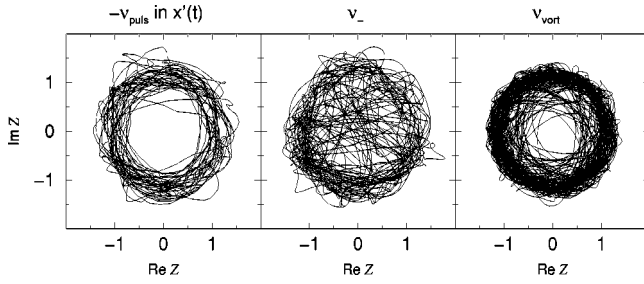


FIG. 8. The trajectories of demodulated, MIRVA filtered signals Z_i (see section 2 of Appendix A), obtained from series B and the quotient signal $x'(t)$, defined in Sec. IV C, at the indicated frequencies. The corresponding values of q_{\min} are 0.30 [$-\nu_{\text{puls}}$ in $x'(t)$], 0.39 (ν_-), and 0.22 (ν_{vort}).

slips in ϕ_{vort} , which broaden the range of relevant frequencies at ν_- and, as a result, worsen the signal-to-noise ratio.

By making use of the MIRVA filtered signal $z_{\text{vort}}(t)$ of the vortex oscillations, ϕ_{puls} can nevertheless be measured from the signal. In variation of a method proposed in Ref. [37], a complex-valued time series $x'(t) := x(t)/z_{\text{vort}}(t)$ is constructed from the original signal $x(t)$. The overall effect of this transformation is to shift all oscillations by ν_{vort} to negative frequencies. The oscillations that were at ν_- are now at $\nu_- - \nu_{\text{vort}} = -\nu_{\text{puls}}$. They are of the form $\sim \exp(-i\phi_{\text{puls}})$, i.e., they do not depend on the phase of the vortices. Now, MIRVA filtering $x'(t)$ at $-\nu_{\text{puls}}$ yields the desired unequivocal phase information (Fig. 8, left). As is shown in Fig. 9, the ϕ_{vort} follows ϕ_{puls} , but several phase slips occur.

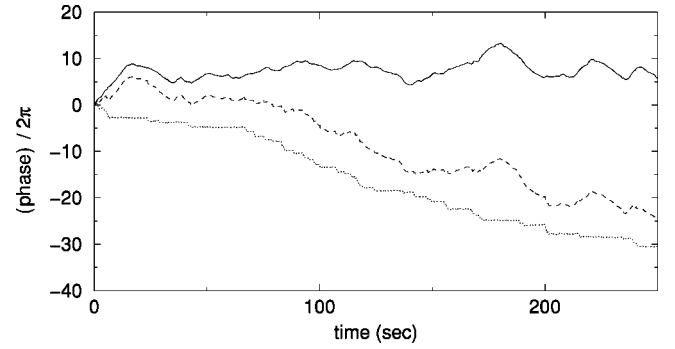


FIG. 9. Unwrapped phases, obtained from series B: $2\phi_{\text{puls}}(t) - \omega_0 t$ (solid) and $\phi_{\text{vort}}(t) - \omega_0 t$ (dashed), where $\omega_0/2\pi = 110.697$ Hz (nominal value); the relative phase $\phi_{1,2} = \phi_{\text{vort}} - 2\phi_{\text{puls}}$ (dotted).

The histogram of the cyclic relative phase $\Psi_{1,2}$ reveals the two preferred phase angles which are due to transversal reflection symmetry (Fig. 10). Since the symmetry is weakly broken, their separation is not exactly π . Again, it is not clear to what degree the broadening of the distribution of $\Psi_{1,2}$ is due to measurement noise and to what degree to internal noise.

2. Quantification of the degree of mode locking

In order to quantify the degree of mode locking independent of measurement noise, a characterization that depends only on the long-term dynamics of the phases would be useful. Such a measure is, for example, given by $\rho_{1,2}$, with

$$\rho_{n,m} := \frac{n^2 D[\phi_{\text{vort}}] + m^2 D[\phi_{\text{puls}}] - D[\phi_{n,m}]}{2m^2 D[\phi_{\text{puls}}]} = \lim_{T \rightarrow \infty} \frac{n \text{cov}[\phi_{\text{vort}}(t+T) - \phi_{\text{vort}}(t), \phi_{\text{puls}}(t+T) - \phi_{\text{puls}}(t)]}{2m \text{var}[\phi_{\text{puls}}(t+T) - \phi_{\text{puls}}(t)]}, \quad (23)$$

where $D[\cdot]$ stands for the diffusion coefficient of the specified phase variable. $\rho_{n,m}$ measures in how far the response oscillator (here vortices) follows phase fluctuations of the drive oscillator (pulsation). When ϕ_{vort} and ϕ_{puls} evolve independently, $\rho_{n,m} = 0$ for all n, m . In the case of hard $n:m$ lock-in, as was found for series A, $D[\phi_{n,m}] = 0$, $n^2 D[\phi_{\text{vort}}] = m^2 D[\phi_{\text{puls}}]$, and $\rho_{n,m} = 1$. Weak mode coupling interpolates between these two extremes. Values of $\rho_{n,m}$ outside the range $[0,1]$ are possible in principle but unphysical in the situation of direct, unidirectional coupling. Since only the long-term dynamics of the phases is taken into account, rather long time series are required to obtain reproducible values of $\rho_{n,m}$. For series B we find, using the estimator given by Eq. (B1) with $\tau = 12.5$ s, $D[\phi_{1,2}] = 0.4(1) \text{ s}^{-1}$, $D[\phi_{\text{vort}}] = 2.4(6) \text{ s}^{-1}$, and $4D[\phi_{\text{puls}}] = 2.5(6) \text{ s}^{-1}$, resulting in $\rho_{1,2} \approx 0.9$. The empirical value of $\rho_{1,2}$ is stable over a wide range in τ . Of course, $\rho_{n,m}$ could not be used when the frequency of the drive oscillator was perfectly stable, i.e., when $D[\phi_{\text{puls}}] = 0$. A detailed analysis

of the measure $\rho_{n,m}$ and its interpretation is yet to be worked out.

V. CONCLUSION

MIRVA filtering was introduced as a method for measuring the phase of oscillations from noisy time series. It was argued that the phase so obtained is, among other favorable properties, particularly robust to noise and linear filtering of the signal. Detailed directions for computing MIRVA filters numerically are given in Appendix A. In a numerical case study it was demonstrated that MIRVA filtering introduces only little bias to the phase (or average) frequency. A synchronization index has been proposed, which is designed to be robust to noise if MIRVA filtering is used.

By applying MIRVA filtering to the signal of a vortex flow meter, we showed that the method can be used to obtain well defined phases from oscillatory time series even under unfavorable conditions such as strong internal and measurement noise. The phases were used to investigate the strength of

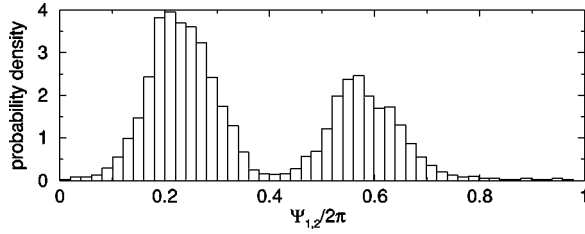


FIG. 10. Empirical distribution function of the cyclic relative phase $\Psi_{1,2}$ obtained from series B. The double peak is a result of the transversal reflection symmetry of the experimental system (Fig. 3).

mode locking. As another application, the MIRVA filtered signal was used for a data driven demodulation technique in Sec. IV C. Limitations to phase measurement, which remain even when MIRVA filters are used, have been addressed.

ACKNOWLEDGMENTS

The authors express their gratitude to F. Buhl and ABB Automation Products GmbH for providing the vortex flowmeter data, to P. Riegler, and Y.-K. The for important comments, and to the German Bundesministerium für Bildung und Forschung (BMBF) for generous support (Grant No. 13N7955).

APPENDIX A: COMPUTATION OF MIRVA FILTERS

1. Main algorithms

In practical applications time series x_i ($i = 1, \dots, N$), sampled from $x(t)$ at evenly spaced discrete times $t = i\Delta t$ are given. The MIRVA filters have to be estimated from this data. Here, two methods are proposed. The first method is more appropriate for short time series, the second is more efficient when N is large. With both methods, the impulse response f_j of the filters is restricted to a finite length M ($j = 1, \dots, M$).

a. Direct method

When using the first method, the convolution

$$z_k = (x * f)_{k+M} = \sum_{j=1}^M f_j x_{k+M-j} \quad (\text{A1})$$

(for $k = 1, \dots, N - M + 1$) is calculated directly, and the expectation values in Eq. (1) are estimated as averages over k . An iterative search algorithm (e.g., a quasi-Newton, soft-line-search minimizer [38]) is used to find the MIRVA filter f_j with $q^2 = q_{\min}^2$.

b. Indirect method

The second method makes use of the fact that q depends on $x(t)$ only through its second and fourth moments. It is often more efficient than the first method but, as a trade-off, entails systematic errors of the order $O(M/N)$ in the estima-

tion of the moments of z_i . For notational convenience, we define the second and fourth moments x_i in the time-discrete representation as

$$c_{ijkl} = \langle x_{\tau-i} x_{\tau-j} \bar{x}_{\tau-k} \bar{x}_{\tau-l} \rangle \quad (\text{A2})$$

and

$$c_{ij} = \langle x_{\tau-i} \bar{x}_{\tau-j} \rangle \quad (\text{A3})$$

with arbitrary τ . These expectation values are estimated by averaging over time and making use of symmetries, e.g., $c_{ij} = \bar{c}_{ji} = c_{i+kj+k}$.

Equation (1) now reads

$$q^2 = \frac{\sum_{ijkl} c_{ijkl} f_i f_j \bar{f}_k \bar{f}_l}{\left(\sum_{ij} c_{ij} f_i \bar{f}_j \right)^2} - 1 \quad (\text{A4})$$

with all sums running over $1, \dots, M$. Thus, while the computation of the moments takes time of order $O(NM^3)$, the time required for the optimization itself is independent of N . Besides, derivatives of q^2 with respect to f_i are calculated at little additional cost, and can be provided to the optimization algorithm to help finding a MIRVA filter f_i .

2. Down sampling, demodulation, and regularization

In order not to introduce artificial restrictions of the search space for f_i , the duration of the impulse response, i.e., $M \times \Delta t$ should be of the order of the phase coherence time of the oscillation. This time can easily cover several hundred oscillation periods. Computation time depends critically on M . To keep M low and make the computation feasible, it is therefore advisable not to work with the raw time series x_i but to perform a demodulation and a down-sampling step prior to the main calculation. For the calculations discussed in Secs. III and IV, instead of x_i , the demodulated time series X_j given by

$$X_j := \sum_l K_l x_{hj+l} \exp[-i(hj+l)\omega_0 \Delta t], \quad (\text{A5})$$

were used with a symmetric, triangular smoothing kernel K_l at a width of two time the down-sampling factor h . The demodulation frequency ω_0 should be set to a value close to the frequency of the targeted oscillations.

To see the effect of this transformation, notice that for stationary, discrete-time processes the value of q defined by Eq. (1) with z replaced by $Z = F * X$ is for any filter F_k identical to the value obtained with $z = f * x$, provided

$$f_k = \sum_l K_l F_{(k+l)/h} \exp(ik\omega_0 \Delta t) \quad (\text{A6})$$

and $F_k := 0$ for noninteger k by convention. It is not difficult to verify that $Z_j = z_{hj} \exp(-ihj\omega_0 \Delta t)$, independent of K_l .

As a result, every MIRVA filter F_k for X_j leads by Eq. (A6) to the approximate MIRVA filter f_k for x_i . The approximation is good if the interpolation (A6) of F_k defined by K_l is reasonable.

The MIRVA filters F_k found for typical experimental data are more or less deformed variants of Gaussian filters $F_k \approx \exp[-\frac{1}{2}(k-M/2)^2 h^2 \Delta \omega^2 \Delta t^2]$ with bandwidth $\Delta \omega$. The linear interpolation for f_k given by the triangular K_l is good if $h \Delta \omega \Delta t \ll 1$. In practice, this requires filter lengths of at least $M \approx 15-30$.

Experimental time series are often not long enough to yield faithful estimates for all $O(M^3)$ independent elements of c_{ijkl} . This problem can be overcome by a regularization of F_k . In our calculations, we restricted the filters F_k to the family $F_k = \exp[P_m(k)]$, with m th order polynomials P_m .

3. A guide to choosing appropriate parameters

The following procedures were used to find appropriate values for the demodulation frequency ω_0 and the down-sampling factor h , which determines the duration of the filter's impulse response $hM\Delta t$. The sampling rate Δt is assumed to be given and M is restricted to a small range by computational limitations.

After an initial guess, the value of ω_0 was set to the value of the empirically found phase frequency ω_{ph} of z_i in an iterative process. In order to adjust h , the envelope $|F_k|$ of the computed MIRVA filter was investigated. When h is too large, $|F_k|$ has a sharp peak and vanishes for all other values. When h is too small, most weight of the filter is concentrated near the end points F_1 and F_M . By inspection one finds $F_1 \approx \pm i F_M$, i.e., the MIRVA filter with a constraint in the filter length approximates a simple 2D delay embedding. h is adjusted accordingly.

A systematic procedure for finding good values for the polynomial order m has not been developed yet. But with $m \approx 6-10$ results generally depend little on the precise value.

4. Convergence and side minima

In Sec. II it was proposed to identify local minima of q with distinct oscillatory components of the signal. The structure of the search space is therefore of immediate theoretical interest. In fact, with long enough time series sampled from a typical signal, the numerical search algorithms used here consistently and effortlessly reach local minima located in a small set of well separated points in the space of all filters, irrespective of the—randomly chosen—starting points. A unique minimum is typically singled out when using demodulation and down sampling, since this effectively implies a preselection of the frequency range of interest. With shorter time series, however, these minima split into large clusters of several side minima. In order to cope with these artificial

multiplicities, only those local minima were accepted for selecting MIRVA filters which were found three times within a series of minimization runs with random starting points, without previously finding any point with a lower value of q .

APPENDIX B: REMARKS ON THE ESTIMATION OF D

We discuss a method to determine the diffusion coefficient D defined by Eq. (14) from samples $\phi(t)$ of finite length ($0 \leq t \leq T$). First ω_{ph} is estimated as $\hat{\omega}_{\text{ph}} = [\phi(T) - \phi(0)]/T$. Then D can be estimated by

$$\hat{D}_\tau := \frac{\int_0^{T-\tau} [\phi(t+\tau) - \phi(t) - \hat{\omega}_{\text{ph}}\tau]^2 dt}{2\tau(T-\tau)(1-\tau/T)}, \quad (\text{B1})$$

where $0 < \tau < T$. The last factor in the denominator compensates for the loss of statistical degrees of freedom by the estimation of ω_{ph} as $\hat{\omega}_{\text{ph}}$. When assuming $\phi(t)$ to perform a random walk with constant drift, it is straightforwardly verified that $\hat{\omega}_{\text{ph}}$ is a maximum likelihood estimator and $\langle \hat{D}_\tau \rangle = D$. Under the same assumption, the variance of $\hat{\omega}_{\text{ph}}$ is $2D/T$ and

$$\text{cov}(\hat{D}_{kT}, \hat{D}_{lT}) = D^2 \frac{l[6(1-k)^2k - 2(1-k)(1+3k^2)l - (1-4k)l^2]}{3k(1-k)^2(1-l)^2} \quad (\text{B2})$$

for $0 < k \leq l \leq 1/2$ (the last expression was obtained with the help of symbolic computer algebra). In particular,

$$\text{var} \hat{D}_{lT} = D^2 \frac{l(4-11l+4l^2+6l^3)}{3(1-l)^4}, \quad (\text{B3})$$

which increases monotonically with $0 < l \leq 1/2$. For good estimates of D , the parameter l should be chosen as small as possible but large enough to justify the assumption of a random walk over times lT . The estimator \hat{D}_τ can be slightly improved by using linear combinations with different τ . For example, the variance of

$$\hat{D}'_\tau := \frac{3}{2}\hat{D}_\tau - \frac{1}{2}\hat{D}_{2\tau} \quad (\text{B4})$$

is about 10% smaller than of \hat{D}_τ , as is verified using Eq. (B2).

-
- [1] A.S. Pikovsky, M.G. Rosenblum, G.V. Osipov, M. Zaks, and J. Kurths, *Physica D* **104**, 219 (1997).
 [2] M.G. Rosenblum, A.S. Pikovsky, and J. Kurths, *Phys. Rev. Lett.* **76**, 1804 (1996).
 [3] P. Tass, M.G. Rosenblum, J. Weule, J. Kurths, A. Pikovsky, J. Volkmann, A. Schnitzler, and H.-J. Freund, *Phys. Rev. Lett.* **81**, 3291 (1998).

- [4] M.G. Rosenblum and A.S. Pikovsky, *Phys. Rev. E* **64**, 045202(R) (2001).
 [5] M.G. Rosenblum, L. Cimponeriu, A. Bezerianos, A. Patzak, and R. Mrowka, *Phys. Rev. E* **65**, 041909 (2002).
 [6] U. Parlitz, L. Junge, W. Lauterborn, and L. Kocarev, *Phys. Rev. E* **54**, 2115 (1996).
 [7] N.F. Rulkov, M.M. Sushchik, L.S. Tsimring, and H.D.I. Abar-

- anel, Phys. Rev. E **51**, 980 (1995).
- [8] B. Schack, P. Rappelsberger, C. Anders, S. Weiss, and E. Moller, Int. J. Bifurcation Chaos Appl. Sci. Eng. **10**, 2565 (2000); J. Bhattacharya and H. Petsche, Phys. Rev. E **64**, 012902 (2001).
- [9] W.J. Freeman, B.C. Burke, and M.D. Holmes, Hum. Brain Mapp **19**, 248 (2003).
- [10] R. Quiñero, A. Kraskov, T. Kreuz, and P. Grassberger, Phys. Rev. E **65**, 041903 (2002).
- [11] A. Stefanovska, H. Haken, P.V.E. McClintock, M. Hozic, F. Bajrovic, and S. Ribaric, Phys. Rev. Lett. **85**, 4831 (2000).
- [12] V.S. Anishchenko, A.G. Balanov, N.B. Janson, N.B. Igoshina, and G.V. Bordyugov, Int. J. Bifurcation Chaos Appl. Sci. Eng. **10**, 2339 (2000).
- [13] B. Blasius and L. Stone, Int. J. Bifurcation Chaos Appl. Sci. Eng. **10**, 2361 (2000).
- [14] J. Bhattacharya, E. Pereda, R. Kariyappa, and P.P. Kanjilal, Sol. Phys. **199**, 267 (2001).
- [15] D.J. DeShazer, R. Breban, E. Ott, and R. Roy, Phys. Rev. Lett. **87**, 044101 (2001).
- [16] S. Boccaletti, J. Kurths, G. Osipov, D.L. Valladares, and C.S. Zhou, Phys. Rep. **366**, 1 (2002).
- [17] A. Pikovsky, M. Rosenblum, and J. Kurths, *Synchronization* (Cambridge University Press, Cambridge, 2001).
- [18] D. Gabor, J. Inst. Electr. Eng. (London) **93**, 429 (1946).
- [19] J.-P. Lachaux, E. Rodriguez, M. le van Quyen, A. Lutz, J. Martinerie, and F.J. Varela, Int. J. Bifurcation Chaos Appl. Sci. Eng. **10**, 2429 (2000).
- [20] P.Y. Ktonas and N. Papp, Signal Process. **2**, 373 (1980).
- [21] J.Y. Chen, K.W. Wong, and J.W. Shuai, Phys. Lett. A **285**, 312 (2001).
- [22] A.G. Rossberg, e-print arXiv.org/physics/0308018.
- [23] M. Arnold, A. Doering, H. Witte, J. Dörschel, and M. Eisel, J. Clin. Monit **12**, 43 (1996).
- [24] K. Josić and D.J. Mar, Phys. Rev. E **64**, 056234 (2001).
- [25] B. Boashash, Proc. IEEE **80**, 520 (1992).
- [26] D.S. Broomhead, J.P. Huke, and M.R. Muldoon, J. R. Stat. Soc. B. Methodol. **54**, 373 (1992); T. Sauer and J. Yorke, Int. J. Bifurcation Chaos Appl. Sci. Eng. **3**, 737 (1993), and references therein.
- [27] J. Guckenheimer and P. Holmes, *Nonlinear Oscillations, Dynamical Systems and Bifurcations of Vector Fields*, Applied Mathematical Sciences, Vol. 42 (Springer, New York, 1983).
- [28] T. Yalçınkaya and Y.-C. Lai, Phys. Rev. Lett. **79**, 3885 (1997).
- [29] J. Theiler and S. Eubank, Chaos **3**, 771 (1993).
- [30] A.G. Rossberg, e-print arXiv.org/nlin.CD/0305038.
- [31] L. Arnold, *Random Dynamical Systems* (Springer, Berlin, 1998).
- [32] H. Risken, *The Fokker-Planck Equation*, 2nd ed. (Springer, Berlin, 1989), Chap. 12, pp. 374–413.
- [33] R.C. Mottram, Flow Meas. Instrum. **2**, 56 (1991); J.E. Amadi-Echendy, H. Zhu, and E.H. Higham, *ibid.* **4**, 225 (1993); M. C. A. M. Peters, E. van Bokhorst, and C. H. L. Limpens (unpublished).
- [34] N.B. Janson, A.G. Balanov, V.S. Anishchenko, and P.V.E. McClintock, Phys. Rev. Lett. **86**, 1749 (2001); N.B. Janson, A.G. Balanov, V.S. Anishchenko, and P.V.E. McClintock, Phys. Rev. E **65**, 036211 (2002); N.B. Janson, A.G. Balanov, V.S. Anishchenko, and P.V.E. McClintock, *ibid.* **65**, 036212 (2002).
- [35] A. Stefanovska and M. Hozic, Prog. Theor. Phys. Suppl. **139**, 270 (2000).
- [36] M. Rosenblum, A. Pikovsky, J. Kurths, C. Schäfer, and P. A. Tass, in *Neuro-Informatics*, edited by F. Moss and S. Gielen, Handbook of Biological Physics, Vol. 4 (Elsevier Science, Amsterdam, 2001), Chap. 9, pp. 279–321.
- [37] H. Gasquet and A.J. Wooton, Rev. Sci. Instrum. **68**, 1111 (1997).
- [38] H. Nielsen, Technical Report No. IMM-REP-0019, IMM, Technical University of Denmark, 2000 (unpublished).